Electronic structure of a grain-boundary model in $SrTiO_3$

Shang-Di Mo and W. Y. Ching
Department of Physics, University of Missouri–Kansas City, Kansas City, Missouri 64110

M. F. Chisholm and G. Duscher
Solid State Division, Oak Ridge National Laboratory, Oak Ridge, Tennessee 37831

(Received 9 November 1998)

It is known that grain boundaries (GB's) in strontium titanate ($SrTiO_3$) play an important and often a controlling role in determining the material's electrical properties. To understand how their electronic structures are related to the GB structures, we have examined two structure models of the $\Sigma 5$ GB in $SrTiO_3$ obtained by first-principles pseudopotential total energy calculations. The electronic structure of bulk crystal and the relaxed GB models are then studied by using the orthogonalized linear combination of atomic orbitals method. Results are presented for the ground-state structural properties and band structure of bulk $SrTiO_3$, the total density of states (DOS), the atom and orbital-resolved partial DOS, effective charges, bond order, charge-density distribution, and near-edge structure of electron energy-loss spectroscopy. It is shown that the GB structures have smaller values of fundamental band gaps, effective charges, and bond orders relative to bulk $SrTiO_3$. There are no GB-induced electronic states within or at the edge of the fundamental band gap. The 100-atom GB model with buckled Sr columns in the GB core is found to be a more likely model. It is also shown that the electron charge distribution across the GB line in $SrTiO_3$ is almost balanced.
[S0163-1829(99)00428-2]

I. INTRODUCTION

Strontium titanate ($SrTiO_3$) is a typical perovskite dielectric with a wide range of technological applications.[1,2] Because of its special properties related to ferroelectricity,[3,4] semiconductivity,[5–9] superconductivity,[10–12] and catalytic activity,[2] strontium titanate has been extensively studied over the years.[3–21] In recent years, the investigations have been extended to the electronic structures of impurities,[15,18] surfaces,[17,18] and electron-doped $SrTiO_3$.[21] More recently, the atomic structure and the electronic properties of grain boundaries (GB's) in $SrTiO_3$ are subjects of great interest[23–30] due to its technological implications.

Polycrystalline $SrTiO_3$ has many applications in electric and electronic devices. The macroscopic properties of many advanced electronic and structural materials are largely determined by the microstructures. In $SrTiO_3$, GBs are responsible for a variety of electrical properties, such as nonlinear current-voltage characteristics.[31,32] It has been suggested that the electrical properties of $SrTiO_3$ can be rationalized in terms of acceptor states at the GB core.[33–35] However, the existence of such GB-induced states has not been clearly demonstrated. The unique electrical properties of polycrystalline $SrTiO_3$ may originate from the segregation of charged defects such as dopants, interstitial atoms, and vacancies to GB. Because a charged GB corresponds to a barrier in electrostatic potential, segregation of charged defects to GBs affects the charge transport properties of polycrystalline $SrTiO_3$. The extent to which point defects segregate to a specific GB depends upon the structure and bonding of atoms at the particular GB. Thus, a systematical study of the relationship between atomic structure and properties of GBs is called for.

By combining the *Z*-contrast imaging and electron-energy-loss spectroscopy in a dedicated scanning transmission electron microscope, the atomic-scale structure and composition at GB's in $SrTiO_3$ with sufficient high resolution have been successfully obtained recently.[23–25] From these experimental results, a unique feature of the $\langle 001 \rangle$ GB core structures has been identified. It has been found that buckled Sr or Ti-O columns exist in these boundaries. These are seen in the $\langle 001 \rangle$ projections of the boundaries as two closely spaced atomic columns.

From a theoretical standpoint, the first step for a detailed investigation on the GB's is to propose a structure model by either *ab-initio* or empirical simulations. The properties of GB's can be calculated based upon the proposed structural model. Additionally, a calculation of the electron-energy-loss near-edge spectroscopy (ELNES) of the $\Sigma 5$ GB in $SrTiO_3$ has been carried by Tanaka *et al.*[26] Their molecular orbital based calculation reproduced the major features of the experimental spectra except for the higher energy peaks. However, the cluster model $(Sr_8Ti_7O_{36})^{28-}$ they used is only an approximate description of the $\Sigma 5$ GB structure in $SrTiO_3$. Recently, the atomic and electronic structure of a $\Sigma 5$ 36.9° (210) $\langle 001 \rangle$ tilt boundary in rutile (TiO_2) has been studied.[36] Two models were studied, one with 60 atoms and the other with 120 atoms in a periodic cell. The calculation confirmed the stability of the proposed atomic model for the GB and provided some insight into the GB electronic structure particularly with regard to the presence and distribution of any new electronic states in the band gap.

In the present paper, we focus on the electronic structure and properties of two structural models of the $\Sigma 5$ GB in $SrTiO_3$ simulated by first-principles pseudopotential plane-wave method.[37] The electronic structure calculation is based on the *ab-initio* orthogonalized linear combination of atomic orbitals (OLCAO).[38] The pseudopotential plane-wave

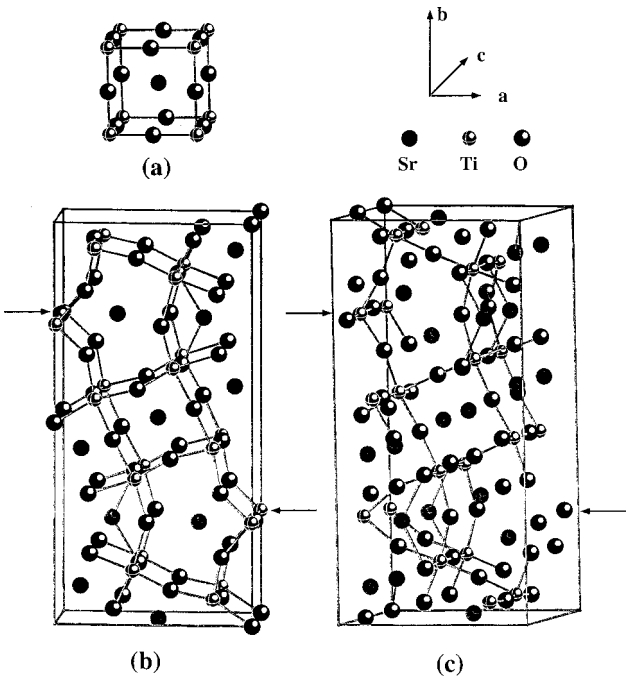

FIG. 1. (a) Crystal structures of bulk $SrTiO_3$, (b) GB50 model, and (c) GB100 model. Arrows indicate the GB lines.

method is known to be accurate and efficient for the structural relaxation of the GB models. The OLCAO method, on the other hand, is very effective in giving accurate self-consistent electronic structures of complex ceramic compounds with large unit cells. The atomistic description of the basis function in the OLCAO method also facilitates the interpretation of interatomic bonding at the GB. A few years ago, the electronic and optical properties of a near edge $\Sigma 11$ GB model in α-Al_2O_3 have been investigated using the OLCAO method.[39,40] The results are in good agreement with experimental data.

The paper is organized as follows. In the next section, we introduce the two proposed GB models in $SrTiO_3$. The electronic property of the bulk $SrTiO_3$ crystal is presented first to demonstrate the accuracy of our method, which can reproduce bulk properties of strontium titanate very well. The calculated electronic properties of the GB models are presented in Sec. IV. A brief summary is given in the last section.

II. ATOMIC CONFIGURATIONS IN $SrTiO_3$ GB

The two structural models of the symmetric 53° $\langle 001 \rangle$ tilt boundary (designated as $\Sigma = 5$ $\{210\}$ $\langle 001 \rangle$ are seen in Fig. 1. Both models are periodic and, therefore, contain two GBs with a three-dimensional supercell. The unit cell parameters *a*, *b*, and *c* are 8.732, 18.024, and 3.905 Å for the 50-atom supercell. The dimension parallel to the tilt axis for the 100-atom cell is 2×3.905 Å. The only difference between the initial configurations of these two models is that the straight Sr column in the GB core of 50-atom model becomes a buckled Sr column in the 100-atom model. The Sr atoms in this column are alternatively displaced towards the adjacent grains.

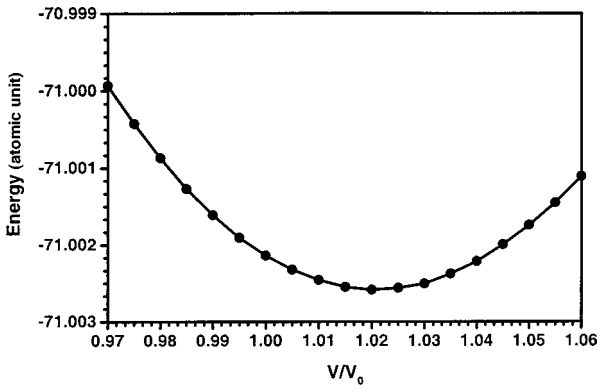

FIG. 2. Calculated total energy of bulk $SrTiO_3$ vs crystal volume.

III. ELECTRONIC STRUCTURE OF BULK $SrTiO_3$ CRYSTAL

The electronic properties of bulk and GB models in $SrTiO_3$ were calculated by using the OLCAO method.[38] A full basis set that includes the minimal basis set (core orbitals plus Sr-5*s*, Sr-4*p*, Sr-4*d*, Ti-4*s*, Ti-4*p*, Ti-3*d*, O-2*s*, and O-2*p*) plus additional excited-state orbitals (Sr-6*s*, Sr-5*p*, Sr-5*d*, Ti-5*s*, Ti-5*p*, Ti-4*d*, O-3*s*, and O-3*p*) was employed. All atomic orbitals are expanded in terms of 21 Gaussian orbitals with exponents ranging from 0.12 to 10^6. The potential and the charge density of the crystal are represented by a superposition of atom-centered functions consisting of simple Gaussians. The Wigner-interpolation formula was used for the exchange-correlation part of the one-electron potential. Twenty, six, and four special *k* points were used in self-consistent iterations for the bulk, GB50, and GB100 models, respectively. The energy eigenvalues and the Bloch wave functions were obtained at 196, 90, and 48 regularly spaced *k* points in the irreducible portion of the Brillouin zone by matrix diagonalization. *Ab initio* wave functions were used to calculate the effective charges, bond order, and partial decomposition of density of states (DOS).

The calculated total energy of bulk $SrTiO_3$ as a function of crystal volume is shown in Fig. 2. The calculated equilibrium lattice constant is 3.931 Å, which is only 0.7% larger than the experimental value.[41] The bulk modulus *B* obtained from fitting the total energy data to the Murnaghan's equation of state[42] is 163 Gpa and the pressure coefficient B' is 3.89. Both the equilibrium lattice constant and the bulk modulus are close to the measured values and the values obtained by other *ab initio* calculations.[17,18] The results are summarized in Table I. Since our calculation gives a good description of the bulk properties of $SrTiO_3$, the same method and procedures were applied to the calculation of GB models in $SrTiO_3$.

Figure 3 shows the calculated band structure of bulk $SrTiO_3$. The top of the valence band (VB) is at the *R* point with energy very close to that of the *M* point. The bottom of the conduction band (CB) is at Γ point and is very close to the *X* point. The upper VB is 5.01 eV wide. The minimal indirect gap between *R* and Γ is 1.45 eV, while the direct gap at Γ is 1.98 eV. The calculated band-gap energy is about half of the experimental value of 3.2 eV.[1] As is well known, this

TABLE I. Calculated ground-state properties of bulk $SrTiO_3$.

	Lattice constant (Å)	Bulk modulus B_0 (Gpa)	Pressure coefficient
This work	3.931	163	3.89
Experimental	3.905[a]	183[a]	
Pseudopotential calc.	3.798,[b] 3.957[c]	194,[b] 166[c]	

[a]Reference 41.
[b]Reference 17.
[c]Reference 18.

discrepancy stems from the local-density approximation (LDA) in the density-functional theory.

The calculated total and atom-resolved partial DOS [partial density of states (PDOS)] of bulk $SrTiO_3$ are shown in Figs. 4(a) and 5, respectively. The major features can be summarized as follows. (i) There are multiple structures in the upper VB. Roughly speaking, three peaks at -1.2, -3.3, and -4.9 eV can be identified. The upper VB is made up predominately of the O-$2p$ components. The peak at -1.2 eV originates from the O-$2p$ nonbonding components, while the other two peaks correspond to the O-$2p$ antibonding combinations of oxygen-oxygen interactions. However, there is a limited Ti-$3d$ contribution in this energy range due to the hybridization with the O-$2p$ states. (ii) The lower VB consists of two parts. The higher one with a single sharp peak at -14 eV is the semicore Sr-$4p$ state. The lower double peak is the O-$2s$ component. The separation energy between the two parts is about 1.26 eV. (iii) The first major peak above the CB edge is contributed mainly by Ti $3d$. This is followed with a more broadened Sr-$4d$ peak in the energy range from 5 to 10 eV. O $3p$ contributes to the high-energy region above 15 eV. All the above features are in good agreement with a recent photoemission spectroscopy study[22] and a linearized muffin-tin orbital calculation.[43]

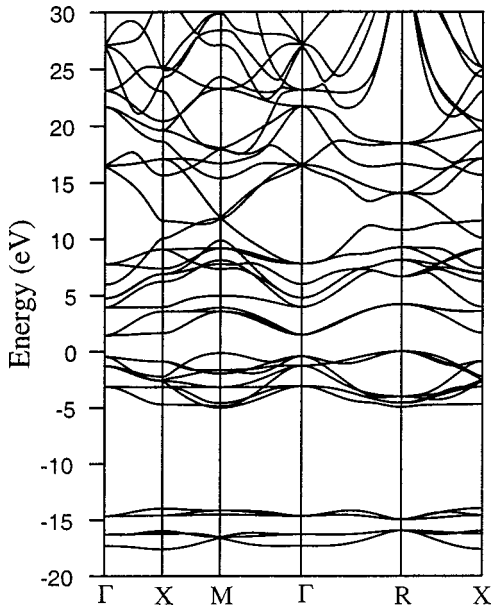

FIG. 3. Calculated band structure of bulk $SrTiO_3$. The zero of energy is set at the top of the valence band.

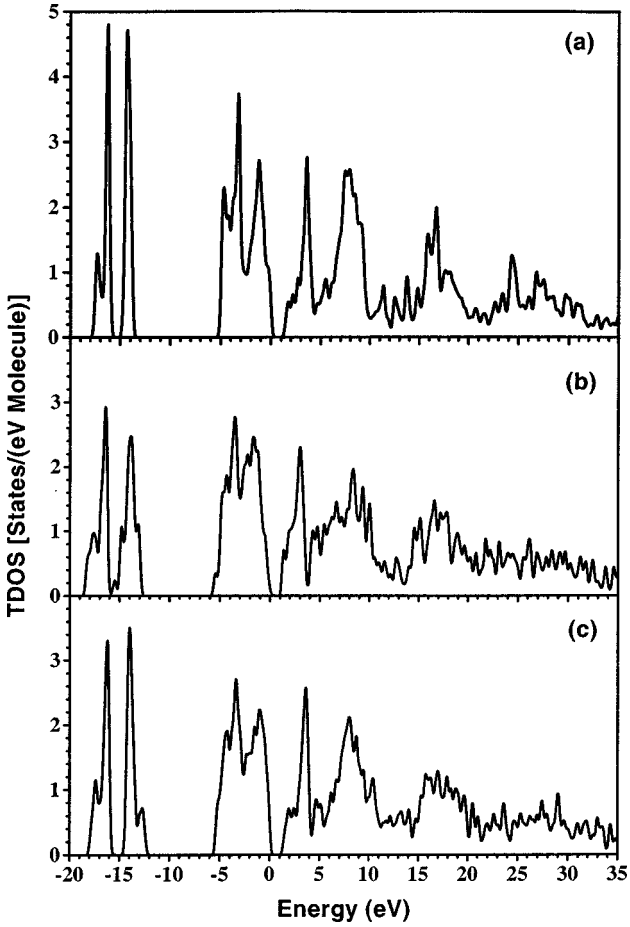

FIG. 4. Calculated total DOS's of (a) bulk $SrTiO_3$, (b) GB50 model, and (c) GB100 model.

Figures 6(a) and 6(b) display contour plots of the calculated valence charge density $\rho(r)$ on the Ti-O and Sr-O planes in bulk $SrTiO_3$. The charge density is highly localized on the oxygen sites and is nearly spherically symmetric. The large concentration of the charge at the O sites is consistent with the highly ionic nature of bulk $SrTiO_3$. Nevertheless, the presence of charge density at the Ti and Sr sites and between the Sr (Ti)-O bond means a substantial covalent bonding character between Sr (Ti) and O. To see the effect of the charge transfer more clearly, the charge density difference $\rho_{\text{bulk}}(r)-\rho_{\text{atom}}(r)$ in the Ti-O and Sr-O planes are plotted in Figs. 6(c) and 6(d), respectively. Figure 6 will be used later as the reference charge density in a similar discussion with the GB models.

IV. ELECTRONIC STRUCTURE OF GB MODELS IN $SrTiO_3$

A. Density of states

The calculated DOS of the GB50 and GB100 models of $SrTiO_3$ are shown in Figs. 4 together with the DOS of bulk $SrTiO_3$. They are quite similar with the peak positions remaining roughly at the same positions. It indicates that no significant changes exist in the bonding due to the presence of the GB. However, subtle differences do exist and they are delineated below: (a) In the lower VB, the Sr-$4p$ and O-$2s$ peaks in the GB models are more broadened. In the GB50

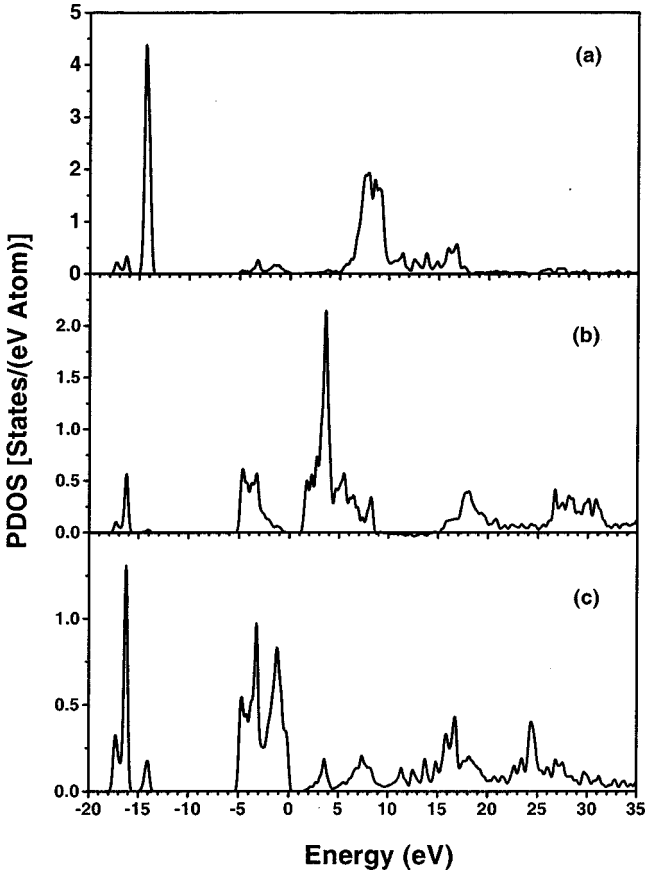

FIG. 5. Atom-resolved partial DOS of bulk $SrTiO_3$: (a) Sr, (b) Ti, and (c) O.

model, the Sr-4p and O-2s peaks are 2.11 and 2.91 eV wide, respectively, while the widths of the same two peaks in the GB100 model are 1.95 and 1.94 eV. In bulk $SrTiO_3$, these two widths are only 0.95 and 1.56 eV, respectively. The Sr-4p peak in the bulk is a sharp single peak. In the GB models, there are multiple-peak structures. This is because the Sr-O bonds are distorted at the GB core. Another noticeable feature is that the Sr-4p peak has slight overlap with the O-2s peak in the GB50 model, indicating a larger distortion than that in GB100. (b) In the upper VB, both the nonbonding and bonding O-2p peaks are broadened and have shoulderlike structures at the lower energy side. As a result, the GB50 and GB100 models have larger upper VB widths of 5.59 and 5.31 eV, respectively, than the bulk. (c) The first major peak in the CB looks similar for the GB models and the bulk. As described before, they are attributed to Ti-3d orbitals. The position and the shape of the Ti-3d peak in the GB100 are closer to those of the bulk. The Ti-3d peak in the GB50 is shifted downward by 1.0 eV. (d) The Sr-4d peaks between 5 to 10 eV in the CB are quite different. The GB models give more broadened structures with many substructures. This is another manifestation of the difference in the Sr-O bonding between the GB models and the bulk. (e) The GB100 model has a direct band gap very close to that of bulk. The band gap of GB50 is indirect and significantly smaller. The smaller band gap is attributed to the more extended feature of O 2p in the VB. The calculated band structure parameters of the GB models and the bulk crystal are summarized in Table II.

B. Charge density

To understand exactly how the bonding at grain boundaries differs from the bonding in the bulk, we examine the

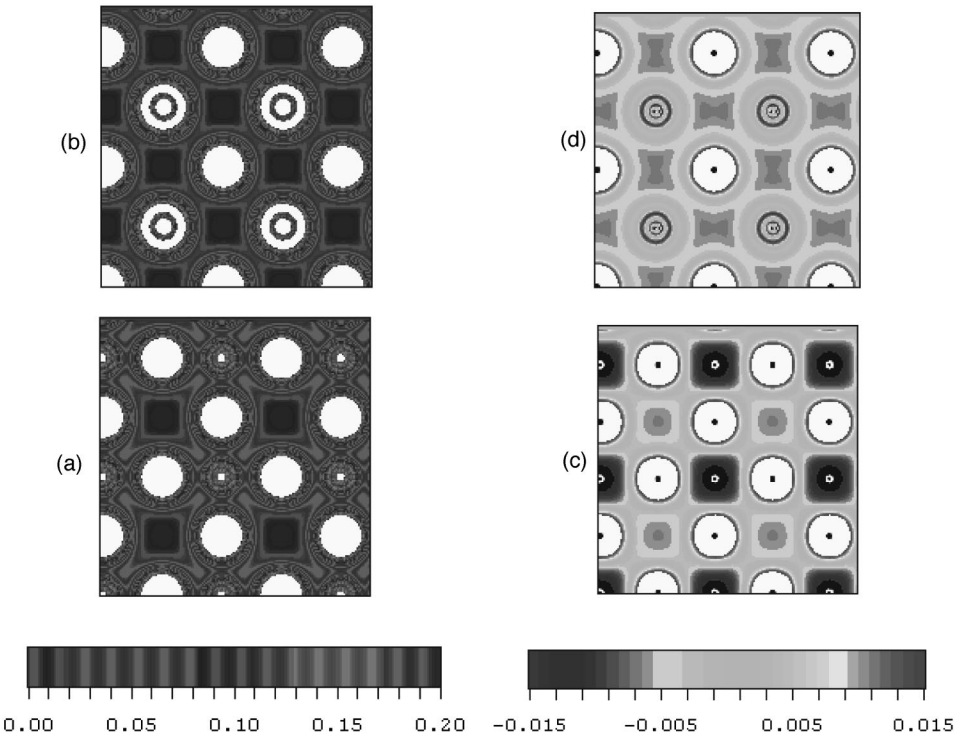

FIG. 6. Charge density of bulk $SrTiO_3$ in (a) Ti-O plane and (b) Sr-O plane. Charge density difference $\rho_{\text{bulk}}(r)-\rho_{\text{atom}}(r)$ between bulk and free atom in (c) Ti-O plane, and (d) Sr-O plane (in units of electrons per cubic atomic unit).

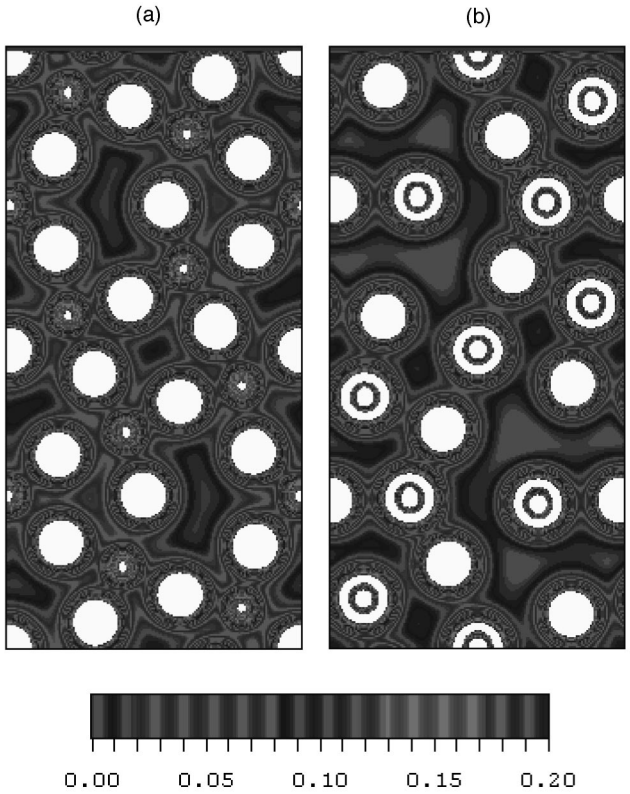

FIG. 7. Charge density of (a) Ti-O plane and (b) Sr-O plane in the GB50 model (in units of electrons per cubic atomic unit). Arrows indicating the GB lines are shown in Fig. 1.

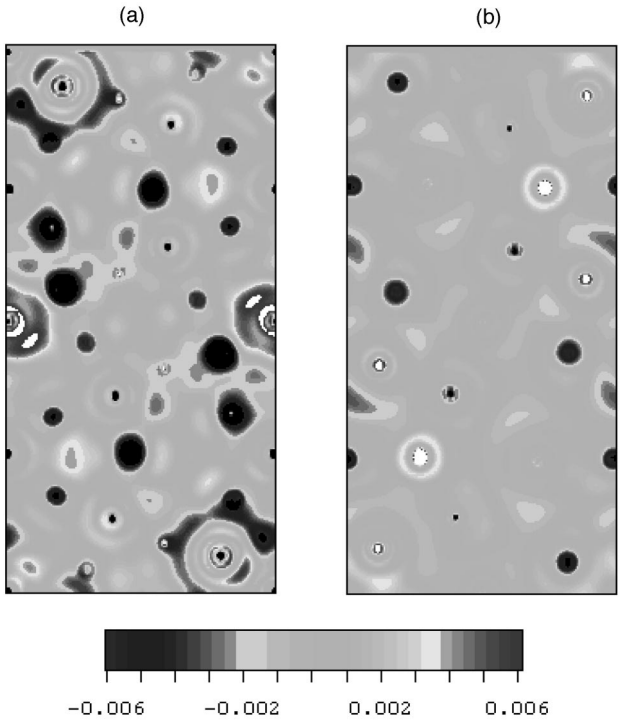

FIG. 8. Charge density difference $\rho_{GB}(r)-\rho_{bulk}(r)$ between GB50 and bulk in (a) Ti-O plane and (b) Sr-O planes (in units of electrons per cubic atomic unit). Arrows indicating the GB lines are shown in Fig. 1.

valence charge distribution and the charge density difference between the GB models and the bulk. Figure 7 shows the charge density on the Ti-O and Sr-O planes in the GB50 model. The differences $\rho_{GB}(r)-\rho_{bulk}(r)$ are shown in Fig. 8. Similar plots for the GB100 model are shown in Figs. 9 and 10, respectively. The charge-density contour maps for the two GB models look similar. The nature of charge distribution in the GB is comparable to the bulk. Subtle differences between the two GB models can be seen at the GB regions. In the Ti-O plane, GB100 has a larger region of low-density distribution at the GB. In the Sr-O plane, the difference between GB50 and GB100 appears to be larger. In GB50, the straight Sr column is in the center of what would be a low-density region.

The distribution of $\rho_{GB}(r)-\rho_{bulk}(r)$ in the GB model provides more information on the charge redistribution at the GB core. These are shown in Figs. 8 and 10 for GB50 and

TABLE II. Calculated band structures of the bulk and GB models in $SrTiO_3$. (ID is indirect band gap and D is direct band gap.)

	O-2s bandwidth (eV)	Sr-4p bandwidth (eV)	Upper VB bandwidth (eV)	Band gap (eV)
Bulk	1.58	0.95	5.01	1.98 (D)
				1.45 (ID)
GB50	2.91	2.11	5.59	1.54 (D)
				1.27 (ID)
GB100	1.94	1.95	5.31	1.42 (D)

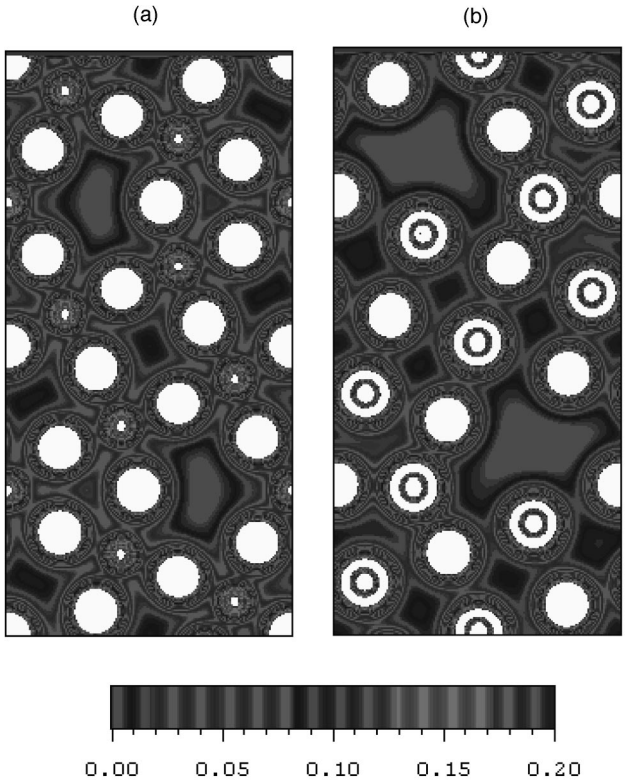

FIG. 9. Charge density in GB100 of (a) Ti-O plane and (b) Sr-O plane (in units of electrons per cubic atomic unit). Arrows indicating the GB lines are shown in Fig. 1.

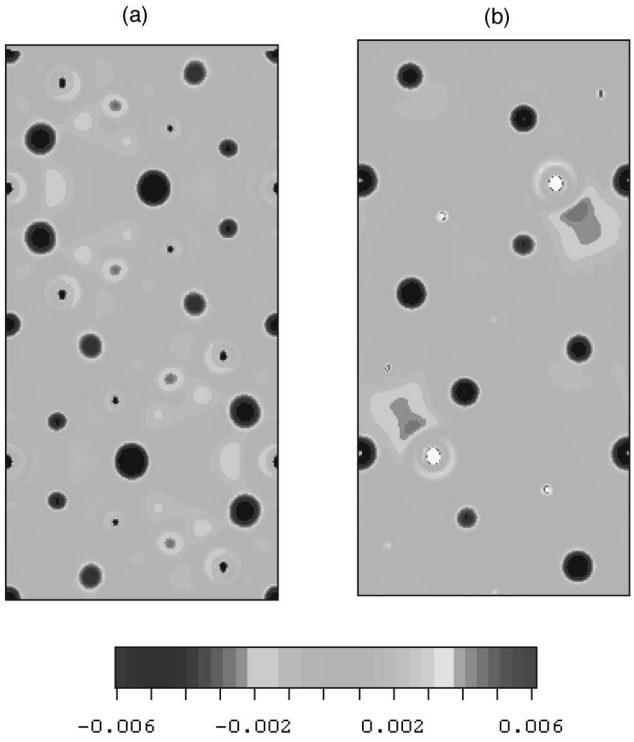

FIG. 10. Charge density difference $\rho_{GB}(r)-\rho_{bulk}(r)$ between GB100 and bulk in (a) Ti-O plane and (b) Sr-O planes (in units of electrons per cubic atomic unit). Arrows indicating the GB lines are shown in Fig. 1.

GB100, respectively. In the Ti-O plane of the GB50 [Fig. 8(a)], there is a relatively large increase in the electron density at O ions away from the GB line with a concomitant relatively large decrease in the density of a nearby ion. On the other hand, there is no such conspicuously large charge difference in the GB100 [Fig. 10(a)]. This may indicate that the straight Sr column in GB50 is somewhat artificial that tends to induce more charge redistribution than the GB100 where the Sr column is buckled. On the Sr-O plane, the difference in charge difference between GB50 and GB100 is less obvious. In the present calculation, there is no indication of charge imbalance across the GB line. The small difference seen in the first of two types of Sr-O plane across the GB is actually balanced out by that in the second Sr-O plane so the net charge imbalance appears to be negligible for the $\Sigma 5$ GB in $SrTiO_3$.

It is important to note that though the DOS's of the GB models are somewhat different from that of the bulk, there are no GB-induced energy levels in or near the fundamental band gap. We have inspected the wave functions of the top most state in the VB and the lowest state in the CB. There is no evidence that these states are specifically related to GB atoms.

The total energy of the GB models was also calculated in the same manner as for the bulk crystal. We find that the GB100 has a slightly lower energy than GB50. However, the high precision required for accurate total energy of a large GB model makes the result on total energy less conclusive.

C. Effective charge and bond order

A simple and effective way to describe charge transfer and chemical bonding is to calculate the effective charge Q_α^* on each ion and the bond order (overlap population) $q_{\alpha\beta}$ between two ions according to

$$Q_\alpha^* = \sum_i \sum_{n,occ} \sum_{j,\beta} C_{i\alpha}^n C_{j\beta}^n S_{i\alpha,j\beta}, \tag{1}$$

and

$$q_{\alpha\beta} = \sum_{n,occ} \sum_{i,j} C_{i\alpha}^n C_{j\beta}^n S_{i\alpha,j\beta}, \tag{2}$$

where $C_{i\alpha}^n$ is the eigenvector coefficient for state n with atomic specification α and orbital specification i. $S_{i\alpha,j\beta}$ is the overlap matrix of the Bloch functions. A separate minimal-basis set calculations of the electronic structure were carried out for the evaluation of effective charges and bond order. It is well known that the Milliken analysis[44] scheme we used is more valid when the basis functions are more localized.

TABLE III. Calculated effective valence charge of bulk and GB models in $SrTiO_3$ (in unit of electrons). Sr-$4p$ electrons are excluded.

Bulk		GB50		GB100	
		Range	Average	Range	Average
Sr	0.90	0.86–1.27	1.00	0.89–1.20	0.98
Ti	3.34	3.08–3.25	3.20	3.33–3.35	3.34
O	6.59	6.32–6.91	6.60	6.53–6.60	6.56

The calculated effective charges for the bulk, GB50 and GB100 are listed in Table III. More (less) than one electron are transferred from Sr (Ti) that indicates a substantial covalent bonding character in the Ti-O bond due to the Ti-$3d$ orbitals. The differences between GB50 and GB100 are consistent with the charge-density analysis in the previous section. The bond order is a qualitative measure of the strength of a bond. In Fig. 11, we plot the bond order against the bond length in the GB models and the bulk. As can be seen, the bond orders in the GB models are smaller than in the bulk. This implies that the bonds are weaker in the GB models. For the GB100 model, the bond order for both Ti-O and Sr-O bonds follows a rough linear relation that the bond order decreases as bond length increases. However, this trend does not fit the GB50 model where the data points are much more scattered. This is particularly evident for the Sr-O bonds. Therefore, the Sr-O bonds are much more distorted in the GB 50 model, which is also responsible for the large variation in the effective valence charges of the Sr ions. It is also the source of the multiple-peak structure in the CB DOS. This provides another additional evidence that the GB 50 model with the straight Sr core column is less realistic than the GB100 model where the Sr column is buckled.

D. ELNES spectra

ELNES is a very effective experimental tool to probe the local chemical environment of atomic-sized imperfections, such as in GB's. It is also well established that atom- and orbital-resolved PDOS in the CB is a reasonable approximation to the ELNES spectra.[45] Recent calculations from our group show satisfactory agreement of the ELNES spectra for

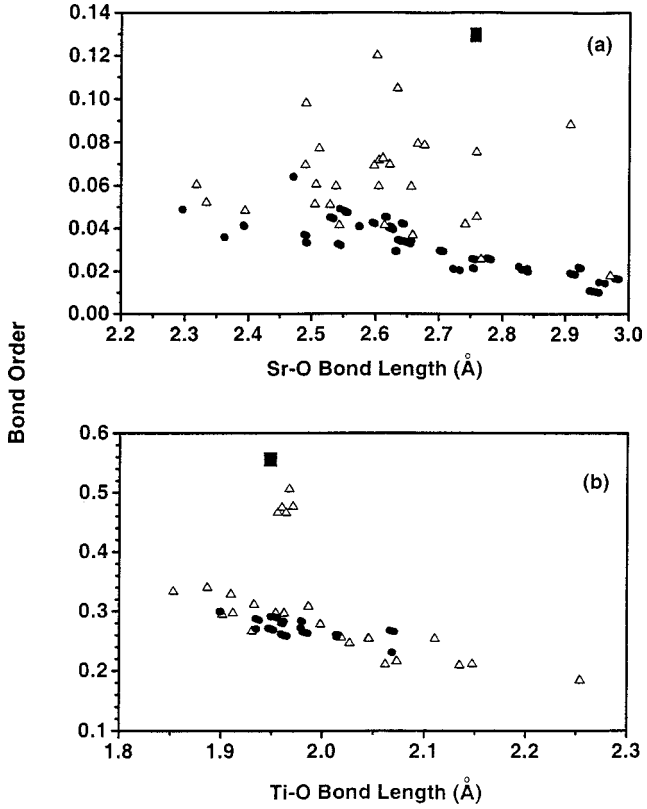

FIG. 11. Bond orders of (a) Sr-O bond and (b) Ti-O bond in GB100 model (solid circles), GB50 model (open triangles), and bulk $SrTiO_3$ (solid squares) vs bond lengths.

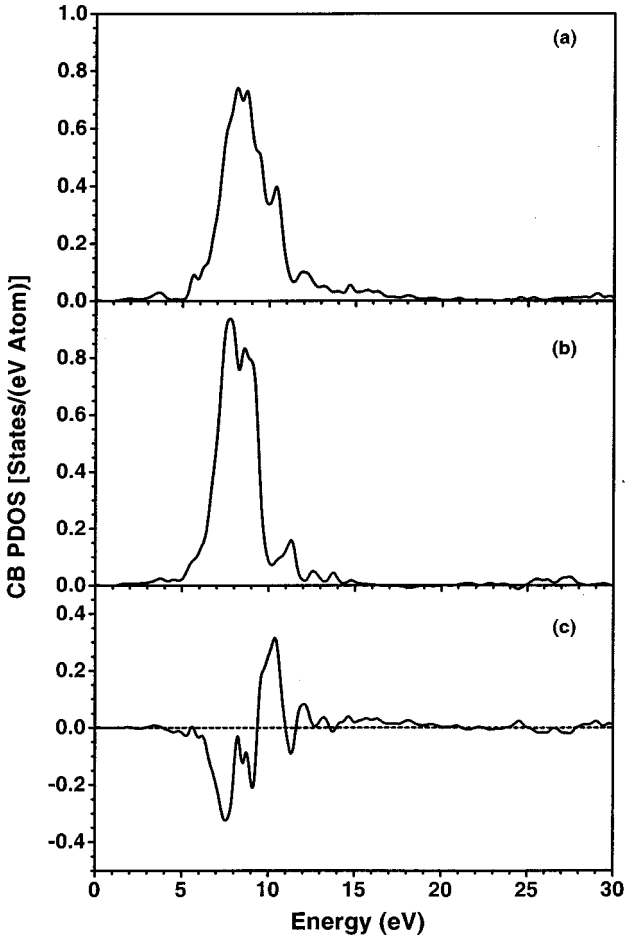

FIG. 12. Partial DOS of Sr $(s+d)$ components for (a) GB100 model, (b) bulk $SrTiO_3$, and (c) difference between (a) and (b).

the Y-Al-O system.[46] In Figs. 12–14, we show the calculated CB PDOS for Sr $(s+d)$, Ti $(s+d)$, and O (p) components. They correspond to Sr-L_{23}, Ti-L_{23}, and O-K edges, respectively. Since we are convinced that the GB100 model is a more realistic one to represent the $\Sigma 5$ GB in $SrTiO_3$, only the data for the GB100 model are shown. Figure 12 shows the PDOS of Sr $(s+d)$ in GB are very different from that of the bulk. The peak position remains the same, but substantial differences occur at the energy ranges below and above the main peak. This is consistent with the more distorted Sr-O bonding at the GB. No experimental Sr-L_{23} spectra are available for comparison. Figure 13 compares the experimental Ti-L_{23} spectra [25] with the calculated PDOS. The experimental spectra was reported on the symmetric $\{920\}\langle 001\rangle$ tilt GB but appeared to be close to the GB models in the present study. For both the GB and the bulk, the calculated PDOS reproduce the higher energy peak at 4 eV reasonably well. For the peak near the absorption edge, the calculation reproduces the peak position, but not the intensity. This is probably due to the core-hole effect at the absorption edge, which was not included in the present study. It has been demonstrated that the Ti-L_{23} fine structure is sensitive to Ti coordination.[47] Figure 13(c) shows the difference in Ti-L_{23} PDOS between GB and the bulk is very small except in the region right next to the main peak. Therefore, it is reasonable to conclude that Ti ions maintain their local coordination across the grain-boundary region. Figure 14 shows the experimental and calculated O-K spectra. At the absorption edge and within the range from 15 to 20 eV, the agreements are reasonable. However, discrepancies exist in the intensity of spectra in the range from 5 to 15 eV. The difference in the O-K spectra between GB and bulk is shown in Fig. 14(c). There is no significant change in peak position and intensity, indicative of no discernable change of oxygen coordination in the GB model.

V. SUMMARY AND CONCLUSIONS

We have investigated the electronic properties of two models of the $\Sigma 5$ GB in $SrTiO_3$. The electronic structure calculations for the bulk and the GB models were carried out by using the first-principles OLCAO method. It is shown that bulk $SrTiO_3$ is a semiconductor with an indirect LDA gap of 1.45 eV. The calculated bulk modulus and pressure coefficient are of 163 Gpa and 3.98, respectively, which are in good agreement with the experiment.

For the two proposed GB models in the $SrTiO_3$, our calculation shows that they have smaller fundamental band gaps, larger widths for the upper VB and lower VB, and smaller effective valence charges than the bulk crystal. DOS calculations suggest that the GB100 model with a buckled Sr column is probably a more realistic model. There is no evidence for the presence of GB-induced energy levels within the fundamental band gap or at the edges of the band gap. Bond-order calculations show that the Sr-O and Ti-O bonding are weaker in the GB region. It is also shown that electron-charge distribution is roughly balanced across the

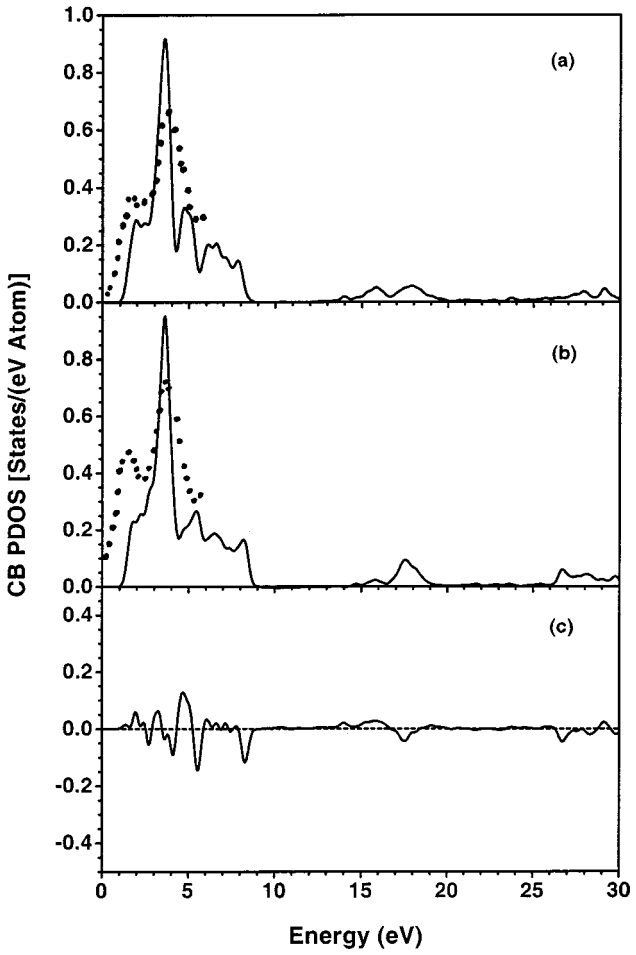

FIG. 13. Partial DOS of Ti $(s+d)$ components for (a) GB100 model, (b) bulk $SrTiO_3$, and (c) difference between (a) and (b). Dotted lines represent the experimental ELNES Ti-L_{23} spectra (taken from Ref. 25).

GB line. The calculated atom- and orbital-resolved partial DOSs in the CB region can reproduce most of the features in the experimental ELNES spectra. The small changes in the Sr-L_{23} spectra indicate a more distorted Sr-O bonding in the GB model in $SrTiO_3$. More realistic calculations should include the core-hole effect and such work is currently in progress. It is also desirable to have GB models of larger sizes and longer repeating units. However, it is unlikely that the main conclusions obtained in the present study will be altered by calculations on larger models. The present method and approach can be extended to cases where impurity atoms are present at the grain boundary. Such studies are not only challenging but are important for real applications.

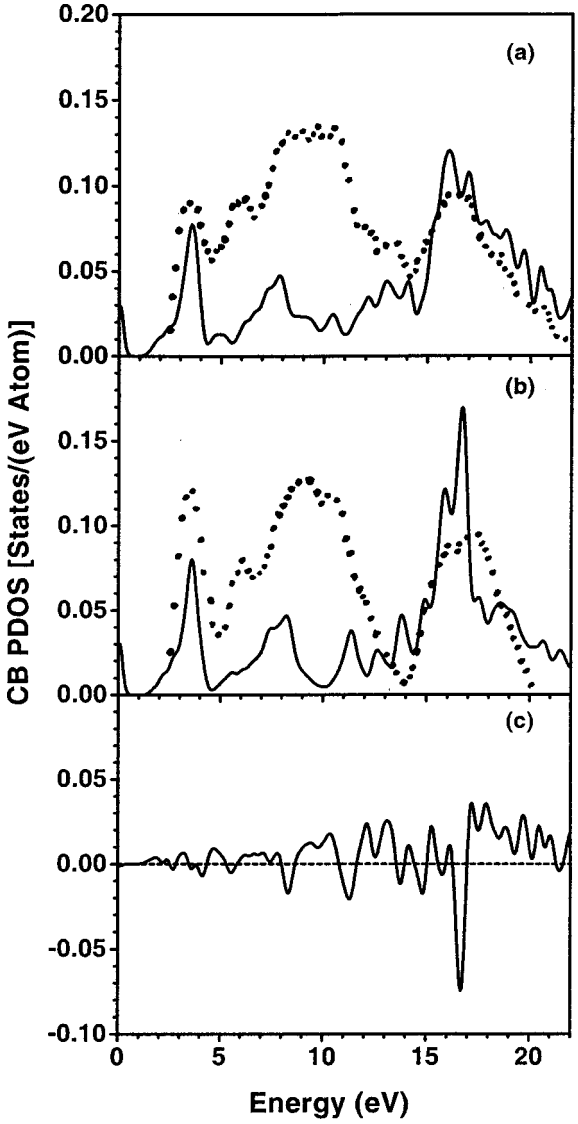

FIG. 14. Partial DOS of O (p) components for (a) GB100 model, (b) bulk $SrTiO_3$, and (c) difference between (a) and (b). Dotted lines represent the experimental ELNES O-K spectra (taken from Ref. 25).

ACKNOWLEDGMENTS

Work at UMKC was supported by the U.S. Department of Energy (DOE) under Grant No. DE-FG02-84DR45170. Work at Oak Ridge National Laboratory was supported by DOE under Contract No. DE-AC05-960R22464 with Lockheed Martin Energy Research Corporation.

[1] M. Cardona, Phys. Rev. A **140**, A651 (1965).
[2] V. E. Henrich, Rep. Prog. Phys. **48**, 1481 (1985).
[3] J. G. Bednorz and K. A. Muller, Phys. Rev. Lett. **52**, 2289 (1984).
[4] F. Gervais, B. Cales, and P. Odier, Mater. Res. Bull. **22**, 1629 (1987).
[5] H. P. R. Frederikse, W. R. Thurber, and W. R. Hosler, Phys. Rev. A **134**, A442 (1964).
[6] U. Balachandran and N. G. Error, J. Solid State Chem. **39**, 351 (1981).
[7] U. Balachandran and N. G. Error, J. Electrochem. Soc. **129**, 1021 (1982).
[8] B. Odekirk, U. Balachandran, N. G. Error, and J. S. Blakemore, Mater. Res. Bull. **17**, 199 (1982).
[9] K. H. Kim, K. H. Yoon, and J. S. Choi, J. Phys. Chem. Solids **46**, 1061 (1985).

[10] J. F. Schooley, W. R. Hosler, and M. L. Cohen, Phys. Rev. Lett. **12**, 474 (1964).
[11] J. F. Schooley, W. R. Hosler, E. Amber, J. H. Becker, M. L. Cohen, and C. S. Koonce, Phys. Rev. Lett. **14**, 305 (1965).
[12] C. S. Koonce, M. L. Cohen, J. F. Schooley, W. R. Hosler, and E. R. Pfeiffer, Phys. Rev. **163**, 380 (1967).
[13] C. Lee, J. Yahia, and J. L. Brebner, Phys. Rev. B **3**, 2525 (1971).
[14] O. N. Tufte and P. W. Chapman, Phys. Rev. **155**, 796 (1967).
[15] M. O. Selme and P. Pecheur, J. Phys. C **21**, 1779 (1988).
[16] Y.-N. Xu, W. Y. Ching, and R. French, Ferroelectrics **111**, 23 (1990).
[17] S. Kimura, J. Yamauchi, and M. Tsukula, Phys. Rev. B **51**, 11 049 (1995).
[18] Z.-Q. Li, J.-L. Zhu, C. Q. Wu, Z. Tang, and Y. Kawazoe, Phys. Rev. B **58**, 8075 (1998).
[19] M. J. Akhtar, Z.-U.-N. Akhtar, R. A. Jackson, and C. R. A. Catlow, J. Am. Ceram. Soc. **78**, 421 (1995).
[20] TH. Guerlin, H. Sauer, W. Engel, and E. Zeitler, Phys. Status Solidi A **150**, 153 (1995).
[21] N. Shanthi and D. P. Sarma, Phys. Rev. B **57**, 2153 (1998).
[22] T. Higuchi, T. Tsukamoto, N. Sata, M. Ishigame, Y. Tezuka, and S. Shin, Phys. Rev. B **57**, 6978 (1998).
[23] M. M. McGibbon, N. D. Browning, M. F. Chisholm, A. J. McGibbon, S. J. Pennycook, V. Ravikumar, and V. P. Dravid, Science **266**, 102 (1994).
[24] N. D. Browning, S. J. Pennycook, M. F. Chisholm, M. M. McGibbon, and A. J. McGibbon, Interface Sci. **2**, 397 (1995).
[25] N. D. Browning and S. J. Pennycook, J. Phys. D **29**, 1779 (1996).
[26] I. Tanaka, T. Nakajima, J. Kawai, H. Adachi, H. Gu, and M. Rühle, Philos. Mag. Lett. **75**, 21 (1997).
[27] O. Keinzle and F. Ernst, J. Am. Ceram. Soc. **80**, 1639 (1997).
[28] O. Kienzle, F. Ernst, and G. Möbus, J. Microsc. **190**, 144 (1998).
[29] O. Keinzle, M. Exner, and F. Ernst, Phys. Status Solidi A **166**, 57 (1998).
[30] R. Feidenhans'l, A. Kazimirov, D. M. Smilgies, Q. Jiang, and J. Zegenhagen, Philos. Mag. Lett. **78**, 51 (1998).
[31] N. Yamaoka, M. Masuyama, and M. Fukai, Am. Ceram. Soc. Bull. **62**, 698 (1983).
[32] M. Fujimoto and W. D. Kingery, J. Am. Ceram. Soc. **68**, 169 (1985).
[33] P. Gaucher, R. L. Perrier, and J. P. Ganne, Adv. Ceram. Mater. **3**, 273 (1988).
[34] Y.-M. Chiang and T. Takagi, J. Am. Ceram. Soc. **73**, 3286 (1990).
[35] S. B. Desu and D. A. Payne, J. Am. Ceram. Soc. **73**, 3391 (1990).
[36] I. Dawson, P. D. Bristowe, M.-H. Lee, M. C. Payne, M. D. Segall, and J. A. White, Phys. Rev. B **54**, 13 727 (1996).
[37] M. C. Payne, M. P. Teter, D. C. Allan, T. A. Arias, and J. D. Joannopoulous, Rev. Mod. Phys. **64**, 1045 (1992).
[38] W. Y. Ching, J. Am. Ceram. Soc. **73**, 3135 (1990).
[39] Shang-Di Mo, W. Y. Ching, and R. H. French, J. Am. Ceram. Soc. **79**, 627 (1996).
[40] Shang-Di Mo, W. Y. Ching, and R. H. French, J. Phys. D **29**, 1761 (1996).
[41] *Numerical Data and Functional Relations in Science and Technology-Crystal and Solid State Physics*, edited by T. Mitsui and S. Nouma, Landolt-Börnstein, New Series, Group III, Vol. 16, Pt. a (Springer, Berlin, 1982).
[42] F. D. Murnaghan, Proc. Natl. Acad. Sci. USA **30**, 244 (1944).
[43] F. M. F. de Groot, J. Faber, J. J. M. Michiels, M. T. Czyżyk, M. Abbate, and J. C. Fuggle, Phys. Rev. B **48**, 2074 (1993).
[44] R. S. Mulliken, J. Chem. Phys. **23**, 1833 (1995).
[45] R. F. Egerton, *Electron Energy Loss Spectroscopy in the Electron Microscope* (Plenum, New York, 1996).
[46] M. A. Gülgün, W. Y. Ching, Y.-N. Xu, and M. Rühle, Philos. Mag. B **79**, 921 (1999).
[47] D. J. Wallis, N. D. Browning, P. D. Nellist, S. J. Pennycook, I. Majid, Y. Liu, and J. B. Vander Sandle, J. Am. Ceram. Soc. **80**, 499 (1997).